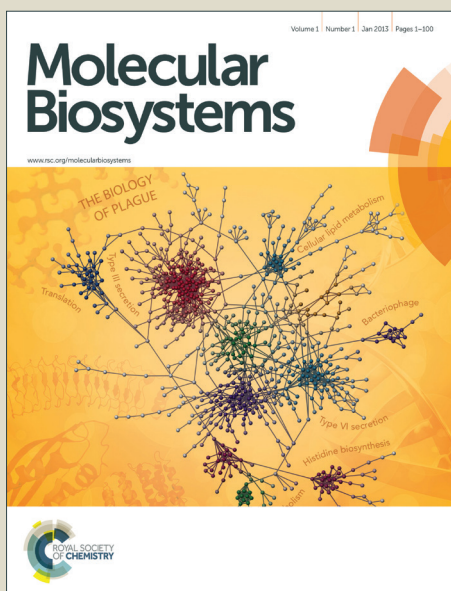


Molecular BioSystems

Accepted Manuscript



This is an *Accepted Manuscript*, which has been through the Royal Society of Chemistry peer review process and has been accepted for publication.

Accepted Manuscripts are published online shortly after acceptance, before technical editing, formatting and proof reading. Using this free service, authors can make their results available to the community, in citable form, before we publish the edited article. We will replace this *Accepted Manuscript* with the edited and formatted *Advance Article* as soon as it is available.

You can find more information about *Accepted Manuscripts* in the [Information for Authors](#).

Please note that technical editing may introduce minor changes to the text and/or graphics, which may alter content. The journal's standard [Terms & Conditions](#) and the [Ethical guidelines](#) still apply. In no event shall the Royal Society of Chemistry be held responsible for any errors or omissions in this *Accepted Manuscript* or any consequences arising from the use of any information it contains.



www.rsc.org/molecularbiosystems

**Conformational Analysis on the Wild Type and Mutated forms of Human
ORF1p: a molecular dynamics study**

Rajagopalan Muthukumaran, Balasubramanian Sangeetha and Ramaswamy Amutha*

Centre for Bioinformatics, School of Life Sciences, Pondicherry University,

Puducherry-605014, India.

* **Corresponding author:** Ramaswamy Amutha, Phone: 00-91-4132654472, Fax: 00-91-4132655211, Email address: amutha_ramu@yahoo.com / ramutha@bicpu.edu.in

Abstract

The protein ORF1p, encoded by LINE-1 retrotransposon, is responsible for the packaging and transposition of its RNA transcript and is reported to involve in various genetic disorders. The three domains of ORF1p co-ordinate together to facilitate transposition and the mechanism of nucleic acid binding is not yet clear. The C-terminal domain of ORF1p adopts either a lifted, twisted or rested state regulated by several inter- as well as intra-domain interactions, and are explored in this study. The residues, Glu147, Asp151, Lys154, Arg261 and Tyr282 are majorly involved in mediating the functional dynamics of ORF1p by forming H-bonds and π -interactions. The importance of these residues was elucidated by performing molecular dynamics simulations on both native as well as mutated ORF1p. The Q147A-D151A-K154A mutant expressed a unique dynamics featuring the lifting motion of the CTD core alone, while R261A mutant resulted in oscillatory motions of CTD. In both cases, the CTDs were held in place by Tyr282 and in its absence, the structural stability of CTDs in the trimeric unit is significantly affected. Additional interactions responsible for stabilizing the trimeric ORF1p to express its native dynamics were extracted in this study. The central role of Tyr282 in maintaining the functional state of ORF1p to facilitate nucleic acid binding and the formation of Ribonucleoprotein complex is well highlighted. The knowledge gained from this study forms the basis for understanding the nucleic acid binding mechanism of ORF1p, which could further provide an additional support in exploring various genetic disorders.

Keywords: ORF1p, CTD, molecular dynamics simulations, retrotransposons, chaperones

1. Introduction

The transposon elements of human genome, comprising about 45% of the genome size, are classified as DNA transposons, long terminal repeat (LTR) retrotransposons and non-LTR retrotransposons¹. The Long Interspersed Element-1 (LINE-1 or L1) belongs to the family of non-LTR retrotransposons and is the only identified autonomously active retrotransposon reported in human genome diversification². The L1 forms about 17% of the total human genome and are found mainly in germ cells and embryos. The retrotransposon replicates by reverse transcribing an RNA intermediate following the Target-primed reverse transcription (TPRT) pathway³, which is distinct from other retrotransposons. TPRT is a process in which, reverse transcription of the RNA intermediate occurs in the nucleus at the point of genome integration. The L1 is 6-7 kb in length and comprises; (i) a 5'-untranslated region (UTR), (ii) two non-overlapping open reading frames (ORF1 and ORF2) and (iii) a short 3'-UTR. The ORF1 encodes a 42 kDa protein (ORF1p), while ORF2 encodes both reverse transcriptase and endonuclease to regulate TPRT⁴⁻⁶. The ORF1p fails to express homology with other proteins and hence its precise role is yet to be resolved. However, studies have reported that, ORF1p is vital for retrotransposition due to its nucleic acid binding and chaperone activities.

ORF1p binds to a single stranded RNA, and specifically expresses strong affinity towards its RNA transcript (*cis*). ORF1p forms a Ribonucleoprotein complex (RNP) to protect its RNA transcript from cellular nucleases^{7, 8}. It is also reported that ORF1p assists in RNA maturation, strand annealing and mismatched base pair correction^{9, 10}. ORF1p consists of 338 amino acids and exists as a trimer¹¹. It is localized to germinal cells, embryos and stress granules in the nucleus^{12, 13}. The ORF1p possesses three structural domains namely, coiled-coil (CC) to mediate homotrimerization, RNA recognition motif (RRM) and C-terminal domain (CTD)⁹. Both RRM and CTD domains facilitate the formation of L1-RNP¹⁴.

The individual structures of RRM and CTD domains were solved by NMR studies^{11, 15}. The trimeric form of ORF1p with all three domains was reported by Khazina et.al in 2011 (PDBID: 2KYO¹⁴) and provides insights into the structural features facilitating both coordination of trimeric form as well as its nucleic acid binding property. The CC is a long α -helical structure with seven heptad repeats within residues Arg49-Val153. In trimer, the CC is held together by leucine zipper motif, inter-chain H-bonds and two Cl⁻ ions (coordinated by Asn142 and Arg135 from all three chains at the second and third heptad repeats, respectively). This trimeric CC assists in maintaining the stability of RRM and CTD domains. Such trimeric coiled coil structure is similar to the trimeric coils of bacterial adhesins as well as viral fibres¹⁶.

The RRM domain (residues Asn157-Asp252) consists of a $\beta\alpha\beta\beta\alpha\beta$ fold, which is located perpendicular to CC axis. The RRM and CC domains are connected by a short linker region (Lys154-Pro156) termed as hinge 1. The CTD (residues Ala255-Met323), that adopts a $\alpha\alpha\beta\beta\beta\alpha\alpha$ fold is anchored to the outside of CC and suspended above the plane of RRM β -sheets. The CTD is connected to RRM by the hinge 2 residues (Leu253 and Ser254). Both hinges 1 and 2 that connect the three domains of ORF1p provides conformational flexibility to the structure. Additionally, the CTD contains an internal hinge (hinge 3) connecting the N-terminal of $\alpha 3$ helix ($\alpha 3N$) with CTD core (Figure 1). The trimeric form of ORF1p is held together by both intra- as well as inter- monomeric H-bonds. The RRM domain is stabilized with respect to the trimeric CC by an intra-chain H-bond between Lys227 and Arg155 as well as an inter-chain H-bond between Asn157 and Tyr152 of adjacent monomers. A three-fold symmetric CC is observed in the crystal structure of ORF1p, which is not expressed by the RRM due its unequal interface contacts. CTD is stabilized by the interactions formed between residues Ser254 and Thr257 of hinge 2 with Gln147, Asp151 and Lys154 of CC-helix $\alpha 0$. An additional π stacking interaction between Tyr282 and Arg155 is also reported¹⁴.

In the crystal structure, the CTD adopts different orientations with respect to the symmetric CC and are referred as 'lifted', 'twisted' and 'resting' positions¹⁴. The 'lifted' position is defined by a $\sim 30^\circ$ upward rotation of CTD domain around hinge2. During this motion, the guanidine group of Arg155 rotates and as a consequence, Tyr282 loses the stacking interaction with Arg155. The 'twisted' position of CTD is characterised by a 45° rotation of CTD core with respect to $\alpha 3N$ helix. In this twisted position, the hydrogen bond between Arg261 (ϵ - nitrogen) and Pro283 (carbonyl oxygen) is lost. Whereas, in resting state, the CTDs do not show any motions and the interactions Tyr282-Arg155 and Arg261-Pro283 are maintained¹⁴. The three domains are arranged in such a manner that it confers increased plasticity to ORF1p and the observed lifted, twisted and resting motions of CTD describe the native dynamics of ORF1p during simulation. Numerous reports are available on the nucleic acid chaperone activity of human and mouse ORF1p, and yet the mechanism of activity remains unresolved. The RNP formation is reported to be essential for retrotransposition¹⁷. Both binding and competitive assay analyses revealed the affinity of ORF1p towards RNA than DNA and in particular, this affinity is more pronounced with single strands than the duplexes (double-stranded DNA, double-stranded RNA or a DNA-RNA hybrid)^{12, 18, 19}. Electrostatic potential surface analysis displays a lining of positively charged residues at the cleft between RRM and CTD, which aids in nucleic acid binding and retrotransposition. The structural dynamics of CTD facilitates nucleic acid binding, such as lifting of CTD opens up the cleft between RRM and CTD to accommodate the nucleic acid backbone rather than the bases.

Mutational analysis provides insights into the structural and functional aspects of ORF1p, and identified three groups of mutations. The first class of mutations (in which the residues Arg235 (RRM) and Arg261 (CTD) lining the RRM-CTD cleft are substituted by Ala) affects the RNA binding [6]. Also mutations at Arg206, Arg210 and Arg211 at the $\beta 2$ -

β 3 loop (RRM) as well as Lys133, Lys137, Lys140 and Arg141 at the lower base of CC are defective in RNA binding. The mutations such as Gln147, Asp151, Lys154, Arg220, Arg261 and Tyr282 affect the structural organization and dynamics of ORF1p and are termed as second class of mutations^{14, 20}. In particular, these mutations disturb the resting position of CTD (Y282A), hinge 1 (R220A), internal stability of CTD (R261A) and the attachment of RRM-CTD linker to CC domain (Q147A-D151A-K154A). The N-terminal truncation (Met1-Glu103) and mutations at Glu116 and Asp123 (CC) are classified as third class of mutants, which neither affects RNA binding nor structural stability. These third class of mutations suggest additional functions of ORF1p such as recruiting other proteins or additional trimers to perform functions beyond nucleic acid binding. The available structural data on ORF1p answers to several questions regarding the domain organization and multimerization, yet the mechanism of nucleic acid binding, chaperone activity and TPRT reaction are to be studied. These characteristic features of ORF1p forms its uniqueness from other non-LTR retrotransposons and viral proteins.

Both conformational flexibility and function are the two inter-linked aspects of a protein. The conformational flexibility that emerge from small-scale side-chain motions to large-scale structural transitions play a vital role in explaining the functional dynamics of a protein and can be measured using both experimental and computational techniques in a time dependent manner²¹⁻²⁴. The classical molecular dynamics methods sample the conformational changes of a biomolecule over a period of time²⁵⁻²⁷. The effect of mutations on biological activity of a protein can be better studied at the atomic level when explored theoretically and in particular, Molecular Dynamics (MD) simulations facilitate extensive analysis²⁸⁻³¹. In this study, molecular dynamics simulation of trimeric ORF1p was performed to gain insights into its structural dynamics. The important interactions responsible for mediating the 'lifted', 'twisted' and 'resting' positions of CTD were analyzed and reported in this study. In addition,

mutations that affect CTD dynamics and the structural integrity were also analyzed by performing MD simulations on mutated trimeric ORF1p (with mutations at R261A, Y282A, Q147A, D151A, and K154A) to understand the importance of these residues in the functional dynamics of ORF1p.

2. Materials and Methods

2.1. Molecular Dynamics Simulations

The crystal structure of trimeric ORF1p with CC, RRM and CTD (PDB ID: 2YKO) was used in this study. The wild type trimeric ORF1p with CTD in resting state was modeled using the chain B of 2YKO and used for further studies¹⁴. The key residues stabilizing the structure of ORF1p (Glu147, Asp151, Lys154, Arg261 and Tyr282) were mutated as alanine in the wild type structure with CTD in resting state. The residues of B and C chains are differentiated with single (') and double (``) quotes, respectively. All atom molecular dynamics simulation was carried out using AMBER 12³² package and ff99SB³³ force field for a period of 50 ns. The wild type and mutated structures were solvated using TIP3P³⁴ water model extending up to 10 Å in all directions from the extents of protein. All the modeled systems were neutralized by adding Cl⁻ ions. The systems were relaxed using steepest descent method followed by conjugate gradient method using a cut-off distance of 10 Å. Long-range electrostatics interactions were treated by particle-mesh Ewald³⁵ procedure. The systems were heated to 300 K over a period of 50 ps at constant volume with a harmonic restraint of 2 kcal/mol/Å² on the protein. The temperature was maintained at 300 K using Langevin dynamics³⁶ with a collision frequency of 2.0 ps⁻¹. All the covalent bonds involving hydrogen atoms were treated with SHAKE algorithm³⁷. The density of the system was relaxed over a period of 90 ps to maintain the pressure at 1 atm. All the systems were equilibrated for 500 ps at constant pressure, followed by an unconstrained production

simulation for a period of 50 ns. The MD trajectories were analyzed using Cpptraj³⁸ module of Amber Tools 13 and 14.

2.2. Cross-correlation analysis

The correlated motions of ORF1p was extracted by the cross-correlation matrix (DCCM), which represents the time-correlated (c_{ij}) behaviour between atoms i and j .

$$c_{ij} = \frac{\langle \Delta r_i \cdot \Delta r_j \rangle}{\langle \Delta r_i^2 \rangle^{1/2} \langle \Delta r_j^2 \rangle^{1/2}}$$

The correlation coefficients are obtained as a matrix in the range of -1 to +1, with the diagonals representing self-correlation³⁹. The positive values indicate motions along the same direction (correlated or co-operative), while negative values indicate motions in the opposite directions (anti-correlated or anti-cooperative). The correlated motions were extracted from the 50 ns MD trajectory of all the simulated systems.

2.3. Principal Component Analysis

The principal component analysis was performed to extract the global mode of dynamics. The covariance matrix (C_{ij}), derived using the atomic fluctuations over the MD trajectory of 50 ns was diagonalized to extract the principal components after removing the translational and rotational motions.

$$C_{ij} = \langle (X_i - X_{i,0})(X_j - X_{j,0}) \rangle$$

The highest eigenvalue represents maximum variation along the corresponding eigenvector, which also provides the direction of atomic motion. The eigenvalues and eigenvectors were extracted using AmberTools 14³⁸ and the modes were visualized using NMWiz plugin of VMD 1.9.1⁴⁰.

3. Results

The three domains of ORF1p namely CC (residues Leu114-Val153), RRM (residues Asn157-Asp252) and CTD (residues Ala255-Met323) domains are connected by two hinge regions such as hinge1 (residues Lys154-Pro156) and hinge2 (residues Leu253-Ser254). These hinge regions are responsible for the structural dynamics of ORF1p namely the ‘lifted’, ‘twisted’ and ‘resting’ motions of CTD. The cyclic and co-ordinated motions of CTD in a trimeric ORF1p are necessary for its nucleic acid binding and chaperonic activities. Mutations affecting the dynamics of ORF1p such as Y282A (lift), R261A (CTD internal stability) and Q147A-D151A-K154A (structural integrity) are considered for this study. The present study focuses on elucidating the structural dynamics of trimeric ORF1p in both wild type and mutated forms using molecular dynamics simulations.

3.1. Molecular dynamics simulations of ORF_{wt}

The structural dynamics of ORF1p trimer in its native form (ORF_{wt}) was simulated for a period of 50 ns and analyzed. The root mean square deviation (RMSD) of ORF_{wt}, calculated as a function of time, stabilizes after 8 ns at an average of 7.96 ± 0.43 Å, during the simulated period (black line in Figure 2(a)). It is also noted that, between 5 to 8 ns, the RMSD rises from 5 to 8.5 Å and reveals major structural changes associated with domain motions. The fluctuation of C α -atoms from their average position is shown in Figure 2(b). The CC domain of all three chains is highly stable, while the CTD show maximum fluctuations. The CTD of chains A and B express higher fluctuation around 6.2 and 9.2 Å, respectively, while the CTD of chain C remains stable. On the other hand, the RRM of chains A and C fluctuate between 1.5 and 4.8 Å, while that of chain B is comparatively stable. The radius of gyration of ORF_{wt} trimer is stable at 29 ± 0.5 Å (black line in Figure 2(c)).

3.1.1. Structural dynamics

In ORF1p, the CTD was observed to be highly dynamic and its motions were extracted from the trajectory of 50 ns. It was observed that, the dynamics of CTD involves dominant lifted, twisted and resting motions with respect to the stable CC and RRM domains (colored blue in Figure 3). These motions of CTDs were analyzed by monitoring the angle and dihedral angle defined by the C α atoms of residues from CC (residues Arg138 and Ser145) and CTD (Leu286 and Leu313). Variations in the measured angle and dihedral angle are shown in Figures 4(a) and 5(a). It is seen that both chains A and B relax until 10 ns and thereafter the CTD of chain A stabilizes at an angle of $95^\circ \pm 3.03$, whereas the CTD of chain B adopts higher angular value ($104.78^\circ \pm 3.53$) than chain A. At the same time, chain C remains constant at $120.83^\circ \pm 3.51$ throughout the 50 ns simulation. The observed reduction in inter-domain angle in chains A and B reflects the lifting of CTD towards CC. When compared to chain A, the lift observed in chain B is partial due to the increase in angle after 10 ns.

Similarly, the dihedral angle between CC (residues Arg138 and Ser145) and CTD (residues Leu286 and Leu313) was calculated and shown in Figure 5(a). During the initial 5 ns of simulation, the dihedral angle of chain A fluctuates and later stabilizes around -5° throughout the simulation period, indicating no prominent twisting motion. The chain B shows a remarkable change in dihedral angle from -5 to $+40^\circ$ during 16 - 20 ns period and further stabilizes at 50° , reflecting a prominent twisting motion. The dihedral angle of CTD in chain C fluctuates around the dihedral values adopted by chain A. These results indicate that the functional dynamics of ORF1p involve in either lifting or twisting of CTD to facilitate nucleic acid binding. The dynamic motions extracted in this study are well in agreement with the experimental observations¹⁴.

3.1.2. Principal component analysis

The dynamics of ORF_{wt} was extracted using PCA and the motion represented by first principal mode (PC1) is depicted in Figure 6(a) using arrows. The trimeric ORF_{wt} structure is colored from blue to red to indicate the variation in fluctuation from the least flexible regions to the most in PC1. Also, the arrows represent the direction and amplitude of motion. All three CCs and RRM of trimeric ORF_{wt} are identified as rigid structures, while only the CTDs express increased fluctuations, reinforcing the observation of RMSF (Figure 2(b)). The CTD of chain A shows a clear lifting motion, which is inclined towards the CC of chain B and not perpendicular to chain A. The CTD of chain B involves in twisting motion towards the direction of chain A. Such twisting motion is expressed by $\alpha 3$ - $\alpha 5$ with respect to $\alpha 3N$, while the hinge 2 and $\beta 5$ -7 act as rigid regions. In contrast to the dynamics of chains A and B, the CTD of chain C is comparatively rigid with less amplitude motion of $\alpha 4$.

3.1.3. Domain motion analysis

The domain motions of trimeric ORF_{wt} were identified using DynDom^{41, 42} by considering the initial and 50 ns simulated structures as the two extreme (initial and final) conformations. The identified hinge regions, fixed and moving domains of all ORF simulations are listed in Table 1. The lifted, twisted and resting motions observed in chains A, B and C, respectively, of ORF_{wt} during PCA analysis are also reproduced in DynDom analysis. Both CC and RRM domains were identified as fixed domain in all three chains, while only the CTDs were identified as moving domains (Supplementary Figure 1(a)). The CTD of chain A is displaced with respect to the fixed domain, for which the residues Asp252-Ser254 act as hinge. For this motion, the hinge axis is nearly perpendicular to the line that joins the centre of mass of both fixed (CC and RRM) and moving domains and hence explains the lifting motion of CTD (closure). At the same time, the CTD of chain B

shows a rotation with respect to the fixed domain, for which the residues Ser254[`]-Glu263[`] (α 3N) act as the hinge region. For this motion, the hinge axis passes nearly parallel to the line joining the centre of mass of both fixed (CC and RRM) and moving domains and hence defines a twisting motion. The CTD of chain C shows a twisting motion as observed in the last 5 ns of MD simulations. The hinge axis for this dynamics was identified as Glu263^{``}-Gly265^{``}. In all three chains, the hinge axes pass within 5.5 Å from the bending residues and hence are termed as effective hinge axes. The residues identified as hinge by DynDom analysis matches well with the experimentally reported hinge residues¹⁴.

3.1.4. Inter- and Intra-chain correlated motions

The inter- and intra- chain correlated motions of trimeric ORF_{wt} were extracted by performing cross-correlation analysis. The correlated and anti-correlated motions are depicted by blue and black shades in Figure 7(a). All three domains show strongly correlated intra-domain motions along with highly correlated CC domains. All three domains of chain A show strong positive correlation with CC and RRM of chain B. The lifting motion of CTD in chain A induces negative correlation with hinge 2 of chain A, CTD of chain B and RRM of chain C. Also, the lifting motion of chain A towards the CC of chain B results in strongly positive correlation. The twisting motion of CTD in chain B results in strong anti-cooperative motion with respect to chains A, B and CC of chain C, whereas, positive correlation is observed with RRM and few regions of CTD in chain C. The chain C does not show vibrant dynamics, which is also reinforced by the reduced intra-domain correlation of CTD.

3.1.5. Interactions stabilizing ORF_{wt}

The trimeric ORF_{wt} expresses strong intra- as well as inter-domain hydrogen bonding interactions during dynamics. The present study analyzes the experimentally reported H-bond

interactions mediating the dynamics of ORF1p trimer (Supplementary Figure 2(a)). The RRM domain is coordinated by CC domain through both intra- and inter-chain H-bonds. The intra-chain H-bond between Lys227 (RRM) and Arg155 (CC) is consistent in chain C, which is weak and fluctuating (from 3 to 4.5 Å) in both chains A and B. Also, the inter-chain H-bond between Asn157 and Tyr152 of adjacent monomers stabilizes the RRMs with respect to the trimeric CC. This inter-chain H-bond is stable at the interface of BC chains, which is weak in AB and AC interface. The dynamics of CTD in chain A and B is directed towards each other and hence imparts a structural asymmetry in the trimer.

The highly flexible CTD interacts with CC and is held in place by H-bonds between residues of α 3N (Ser254, Thr257) and CC (Glu147, Asp151, and Lys154). The H-bonds Gln147-Thr257, Asp151-Ser254 and Asp151-Thr257 remain stable only in chain C and retain the CTD in resting state. In both chains A and B, these interactions are disturbed after 5 ns simulation as a result of CTD dynamics, while Lys154 forms weak interaction with Asp252 and Leu253. The Gln147-Thr257 H-bond forms intermittently in chain B after ~22 ns and might be responsible in stabilizing α 3N to facilitate the rotation of CTD core. Initially, the trimeric ORF_{wt} was modeled as a symmetric structure with all three CTDs in resting position and the monomers are held together by strong H-bonding interactions between the CC domains. In addition to these interactions, the trimer also shares inter- monomeric interactions between RRM and CTD via the H-bonds. After 50 ns simulation, an asymmetric behaviour is observed due to the relaxation of both RRM and CTD during dynamics and hence the AC, AB and BC interfaces experiences either less or more H-bonds among themselves as listed in Supplementary Table 1.

Few interactions which are responsible for the lifting and twisting motions of CTD such as π -interaction of Tyr282 with Arg155 and H-bond interaction between Arg261 and Pro283 have been reported. The π -interaction is measured by calculating the distance

between the centroid of Tyr282 phenyl ring (positioned at the loop connecting $\beta 5$ and $\beta 6$) and the side chain NH1 atom of Arg155 (hinge 1) and is shown in Figure 8.I(a). In chains A and B, the residues involving in π -interaction move apart and the distance increases from 5 to 13.4 ± 1.9 and 18.9 ± 0.7 Å, respectively, due to the lifting and twisting motions of CTD. On the other hand, the π -interaction in C chain is maintained throughout the simulation period of 50 ns with an average distance of 4.4 ± 0.4 Å. The twisting motion of CTD is characterized by the rotation of CTD core and disrupts the H-bond between Arg261 ($\alpha 3N$) and Pro283 (loop connecting $\beta 5$ and 6). The H-bond distance was monitored between N_e -atom of Arg261 and backbone O-atom of Pro283 to confirm the twisting motion of CTD (shown in Figure 9(a)). This H-bond interaction remains stable in chains A and C with an average value of 3.08 ± 0.3 Å and 2.96 ± 0.1 Å, respectively and signifies the absence of twisting motion. On the contrary, this H-bond is highly disturbed in chain B with an average distance of 4.22 ± 0.7 Å and as a consequence, a prominent rotation of CTD is observed. In addition to these experimentally reported H-bonds, additional H-bonds are involved in stabilizing the trimer and facilitate the dynamics of ORF_{wt}. During the lifting motion of CTD, a network of H-bonds are formed at the CTD-CC' interface involving residues, Glu256, Gln259, Arg141' and Glu143. When Gln259 establishes a H-bond with Arg141', further lifting of CTD is facilitated as seen in chain A. Altogether, the H-bonds Glu256-Arg141' and Gln147-Thr257 stabilize $\alpha 3N$ to facilitate the free dynamics of CTD core. Additional H-bonds stabilizing and mediating the lifting and twisting dynamics of CTD have also been identified through the present analysis. The CTD of chain A (Gln301 and Arg304) forms H-bonds with CC (Glu136) as a consequence of the lifting motion. Initially, Tyr282 does not involve in any H-bond interactions, whereas, during simulation, it expresses H-bond interaction with CC or RRM according to the CTD dynamics. When CTD is maintained in the resting state, Tyr282'' interacts with Asp151'' of CC as observed in chain C. During the twisting motion of

CTD in chain B, the π -interaction (Tyr282`-Arg155`) is disturbed and the rotation further leads to the formation of a H-bond between Tyr282` and Val251`. The twisting motion of CTD in chain B occurs during 16-20 ns simulation period and the Tyr282`-Val251` H-bond is formed only after 19 ns (Figure 8.II(a)). Hence, it can be assumed that the interaction of Tyr282` with Val251` of RRM stabilizes the position of CTD core. The lifting motion of CTD exposes the cleft between CTD and RRM and consequently, Tyr282 could not express any H-bond interactions with either CC or RRM. This observation is also revisited by chain A. Thus it can be inferred that, Tyr282 regulates the dynamics of CTD such as lifting, twisting and resting motions.

3.2. Mutations affecting the functional dynamics of trimer

The residues Tyr282 and Arg261 are responsible for the functional dynamics of ORF1p such as internal stability (Arg261) and lifting motion (Tyr282) of CTD. Mutations of these residues disrupt the important interactions regulating CTD dynamics and render the ORF1p in an inactive state. Hence, the residues Tyr282 and Arg261 were mutated to Alanine and the mutated systems (referred as ORF₂₈₂ and ORF₂₆₁, respectively) were subjected to molecular dynamics simulations for a period of 50 ns in order to understand their importance in CTD dynamics.

3.2.1. Structural dynamics of ORF₂₆₁

The RMSD of ORF₂₆₁ gradually stabilizes after 15 ns with an average value of 7.7 ± 0.5 Å, which is closer to the RMSD of ORF_{wt} (red line in Figure 2(a)). When the atomic fluctuations of C α -atoms are considered, the RRM of B & C chains and CTD of A & C chains show increased fluctuations than ORF_{wt} (red line in Figure 2(b)). The Rg of ORF₂₆₁ increases consistently up to 30.38 Å during the initial 14 ns and later stabilizes with an

average value of $29.52 \pm 0.3 \text{ \AA}$ (Figure 2(c)), which is also closer to ORF_{wt}. These results indicate that ORF₂₆₁ does not experience major conformational changes during the simulation period (colored light blue in Figure 3).

The structural dynamics of ORF₂₆₁ was analyzed by monitoring the lifting, twisting and resting motion of CTD. The variation in the inter-domain angle between CC and CTD is shown in Figure 4.II(a). The dynamics of chain A is distinctly observed as two phases. In the first phase (during the initial 14 ns), the angle between CC and CTD decreases up to 90° and in the second phase, it relaxes to 80° until 32 ns and stabilizes thereafter. Whereas, in chain B, the angle decreases to about 100° during 16 ns simulation period and remains stable with an average angle of $100.5 \pm 2.7^\circ$. The angle in chain C increases about 20° from the initial value during the first 20 ns of simulation and reverts to the initial state during the rest of the simulation period. The decrease in angle signifies the lifting motion of CTD towards CC, while the increase reflects a closure motion of CTD towards RRM. The absence of H-bond between Arg261 and Pro283 results in an irregular twisting behaviour which is reflected in the measured dihedral angle between CC and CTD. Figure 5.II(a) clearly depicts the lack of prominent twisting motion in both chains A and B of ORF₂₆₁, as the dihedral angle oscillates with respect to the equilibrium position.

The first principal mode of dynamics of ORF₂₆₁ is shown using arrows in Figure 6(b). The CTDs of all three chains show a lifting motion. This motion in chain A is perpendicular to CC, whereas the same in chain B is inclined towards the CC of chain C. In chain C, the inter-domain angle identifies a closure motion, which relaxes back to the initial state after 20 ns and hence the extracted PC1 indicates the lifting of CTD during dynamics. All these dynamic motions are distinct when compared to the characteristic dynamics observed for ORF_{wt}. The R261A mutant leads to an oscillatory motion of CTD and hence, only the lifting motion is seen in the PC1 as the prominent dynamics. In addition, the CCs of chains A and B

along with RRM of chains B and C show dynamic behaviour, which is absent in ORF_{wt}. The RRM of chain B moves towards CTD of chain C, whereas the RRM of chain C moves freely.

The hinge residues for these dynamics were extracted using DynDom and are reported in Table 1. The hinge region for the dynamics of both chains A and B is located at the experimentally reported hinge 2 (Leu253-Ala255), which facilitates the lifting motion. Also, the identified hinge axis is the effective hinge axis for the lifting motion as it passes within 5.5 Å from any bending residues. Whereas in chain C, the residues Ala261-Glu263 were identified as hinge and indicate a twisting motion. This is an improper twisting motion since the hinge axis passes quite away (> 5.5 Å) from the hinge region (Supplementary Figure 1(b)).

The correlated and anti-correlated motions among the three chains of ORF₂₆₁ were extracted using cross-correlation analysis and is shown in Figure 7(b). The intra-domain motions become highly correlated in ORF₂₆₁ than ORF_{wt}. The CC and RRM coordinate together as a single domain in all three chains and show strong inter-chain correlated motions. The CTD of all three chains expresses strong anti-correlation with other domains and in particular, all these CTD domains move in-concert with each other due to its oscillatory behaviour. Since the lifting motion of CTD is perpendicular towards the respective CC, the positive correlation with CC (as observed in ORF_{wt}) is absent in ORF₂₆₁. All these analyses reinforce the divergent dynamics of ORF₂₆₁ in comparison with ORF_{wt} and specifically highlight the instability of CTD dynamics due to mutation at Arg261.

3.2.1.1. Interactions stabilizing ORF₂₆₁

The intra- and inter- chain H-bonds (such as Lys227-Arg155 and Asn157-Tyr152, respectively) stabilizing both CC and RMM domains were monitored in ORF₂₆₁. The H-bond between residues Lys227 (RRM) and Arg155 (CC) oscillates between 2.5 and 5.5 Å

in all three chains, while the H-bond between Asn157 and Tyr152 stabilizes only the CA interface during dynamics. The H-bonds, such as Asp151-Ser254, Asp151-Thr257, Gln147-Thr257 and Lys154-Asp252, that hold CTD closer to CC, are observed only in the initial 5 ns of simulation and are disturbed in all three chains when CTD undergoes a dynamics comprising lifting and oscillatory motions (Supplementary Figure 2(b)). Due to the dynamic nature of CTD, the π -interaction between Tyr282 and Arg155 is also absent in all three chains (Figure 8(b)). As observed in the ORF_{wt}, the AC, AB and BC interfaces also experiences more number of H-bonds due to the relaxation of both RRM and CTD during dynamics (Supplementary Table 1).

The H-bonds which regulate CTD dynamics apart from the reported interactions were also extracted. In ORF₂₆₁, Tyr282 interacts with Asp252 (in chains A and B) and Asp151 (in chain C) and their variation is shown in Figure 8.I and II(b). In chain A, Tyr282-Asp252 H-bond is present only during the initial lifting phase (between 18-32 ns), while in chain B, it is observed after the lifting and oscillatory motions of CTD (from 14 ns onwards). It was observed from ORF_{wt} that, Tyr282-Val251 interaction stabilizes the CTD core. Val251 is located in the β 1 of RRM while Asp252 connects RRM and hinge2. In the initial conformation, the distance from Tyr282 to Val251 and Asp252 is 12.3 Å and 8.2 Å, respectively. Hence, in order to interact with Val251, the CTD core (Tyr282) must experience a rotation. Whereas, for the Asp252-Tyr282 interaction, the in-plane location of Asp252 could easily express H-bond with Tyr282 as the CTD undergoes an oscillatory motion during dynamics (i.e. as observed in the A and B chains of ORF₂₆₁). On the other hand, the CTD of chain C does not show any lifting motion due to the variable interactions of Tyr282 with Gln144 (H-bond) and Lys154 (π -interaction). Additional interactions between residues Leu286, Ser287 and Glu293 of CTD in chain C and the residues of RRM in chain B such as Arg206 and Tyr207 stabilize the CTD of chain C. All these analyses highlight the

role of Tyr282 in regulating the dynamics of CTD during the absence of Arg261-Pro283 interaction.

3.2.2. Structural dynamics of ORF₂₈₂

The RMSD of ORF₂₈₂ stabilizes after 14 ns at $13.14 \pm 0.7 \text{ \AA}$, which is higher than ORF_{wt} (Figure 2(a)). Such higher RMSD fluctuation is the consequence of high amplitude dynamics of both RRM and CTD domains as evidenced by their RMS fluctuations (Figure 2(b)). Accordingly, within the initial 10 ns, the Rg value of ORF₂₈₂ also increases from 30 to 35 \AA and explains its less compact nature than other mutated systems (Figure 2(c)). The high RMSD, RMSF and Rg values of ORF₂₈₂ could be the result of large conformational changes.

Tyr282 is responsible for maintaining the orientation of CTD with respect to both CC and RRM. Y282A mutant fails to provide the necessary leverage for CTD and hence the native dynamics of CTD is completely affected (colored magenta in Figure 3). The lifting, twisting and resting states of CTDs in all three chains were analyzed by monitoring the inter-domain angles and dihedrals using the reference residues as considered in ORF_{wt}. The B and C chains show lifting motion after 20 ns associated with the angular values of $109.9 \pm 9^\circ$ and $95.8 \pm 5.6^\circ$, respectively, while chain A shows only a partial lift characterized by an angle of $110.97 \pm 4.3^\circ$ (Figure 4.I(b)). The inter-domain dihedral angles demonstrate increased fluctuations in both B and C chains, while it is stable in chain A (Figure 5.I(b)). It is assumed that the lack of Tyr282-Arg155 π -interaction that stabilizes CTD leads to such high amplitude dynamics of CTD.

The motion along PC1 derived using PCA is shown in Figure 6(c). Due to the absence of Tyr282, the CTDs are unable to retain its interaction with CC or RRM and hence move away from the CC axis. In PC1, the chain B moves away from the CC axis, while the chain C moves towards chain A with high amplitude. In contrast to this, CTD of chain A does not

show a dynamic behaviour. The hinge residues for such dynamic CTDs were extracted using DynDom and listed in Table 1. Since all three chains express improper native state dynamics, the predicted hinge residues were not similar to ORF_{wt} or the experimentally identified hinge residues (Supplementary Figure 1(c)).

The correlated motions in ORF₂₈₂ extracted using cross-correlation analysis is shown in (Figure 7(c)). The intra-domain correlations are highly increased in ORF₂₈₂. All three domains of chain A show strong correlation and behave as a single domain. In particular, the CC domains involve in a strong co-operative motion. The CTD of B and C chains show anti-correlated motion with the rest of the domains in the trimer and the observed anti-cooperativity is due to motion of CTD away from the CC. In general, the dynamics of CTDs in ORF₂₈₂ is significantly different from the dynamics in ORF_{wt} and ORF₂₆₁.

3.2.2.1. Interactions stabilizing ORF₂₈₂

In ORF₂₈₂, the H-bond between Lys227 and Arg155, which is responsible for stabilizing the orientation of RRM with respect to CC is stabilized at 3.3 ± 0.5 , 3.1 ± 0.4 and 3.1 ± 0.5 Å, respectively in all the three chains. The inter-chain H-bond between Asn157 and Tyr152 is weak at CB and BA interfaces, while it is completely absent at AC interface. All the interactions between CTD and CC are highly disturbed in both B and C chains, while in chain A, the H-bond, Lys154-Asp252 is formed at a distance of 3.17 Å. (Supplementary Figure 1(c)). The influence of CTD dynamics on the trimeric ORF₂₈₂ is reflected from the variable no of H-bonds observed at the AC, AB and BC interfaces (Supplementary Table 1)

The CTDs of B and C chains are displaced from the trimeric CC and hence, do not form any H-bond interactions. The residues of hinge2 and α 3N were identified as hinge for the CTD dynamics in these chains. Hence, the Arg261-Pro283 H-bond is absent in chain B and show weak interaction in A and C chains (shown in Figure 9(b)). The residues of CTD in

chain A (residues Ser281, Ala284, Glu291, Glu293, Ile294 and Tyr296) form 7 alternating H-bonds with residues Arg206^{''}- Arg210^{''} of RRM in chain C and hence does not show any lifting motion or displacement from CC. In turn, this loop (Arg206^{''}- Arg210^{''}) is stabilized by H-bonds with the respective CTD (Ser208^{''}-Glu273^{''} and Ser209^{''}-Lys272^{''}). Such network of H-bonds holds the CTD of chain A as highly stable. Due to the mutation at Tyr282, the characteristic interactions of Tyr282 with residues such as Asp151, Val251 and Asp252 are absent.

3.3. Mutations affecting the structural integrity

Apart from the mutations that affect the functional dynamics of ORF1p, mutations at the residues Glu147, Asp151 and Lys154 of CC are reported to affect the structural integrity of trimeric ORF1p. Hence, these residues Glu147, Asp151 and Lys154 were mutated to Alanine (ORF_{tri}) in the ORF_{wt} structure and simulated for a period of 50 ns.

3.3.1. Structural dynamics of ORF_{tri}

Among the studied systems, ORF_{tri} is observed as the most stable structure having the RMSD at 4.8 ± 0.6 Å (Figure 2(a)). Accordingly, the RMS fluctuation of ORF_{tri} (Figure 2(b)) is also lesser than other systems and the CTD in chain C only expresses an increased fluctuation. As a consequence of the stable dynamics, ORF_{tri} possesses a compact Rg value of 28.4 Å (Figure 2(c)).

The dynamics of CTD was analyzed by measuring the angles and dihedral angles using the reference residues as considered in ORF_{wt}. The angles are stable in A and B chains and is shown in Figure 4.II(b). After 30ns, the angle in C chain decreases to 98.7 ± 2.6 °, which indicates a partial lifting motion as observed in chain B of ORF_{wt}. The dihedral angle between CTD and CC was monitored to analyze the twisting motion in CTD and the

variation is shown in Figure 5.II(b). The dihedral angle of B chain is stable throughout the simulation. The A and C chains show variation in the dihedral angle, however, no distinct changes are observed as seen in chain B of ORF_{wt} (Figure 5.II(b)).

The first principal mode extracted using PCA is shown in Figure 6(d). All three chains show lifting motion, while the chain C expresses high amplitude motion than other chains. The PC1 discloses no explicit twisting motions during dynamics. During the period of simulation, all these motions are not in agreement with the native state dynamics and the predicted hinges using DynDom analysis also reflect this observation (Table 1). The residues Val251-Leu258 (hinge2 as well as α 3N), act as the hinge for the dynamics of CTD in both B and C chains (Supplementary Figure 1(d)).

The ORF_{tri} expresses less amplitude motions between the domains as well as chains, when compared to other studied systems (Figure 7(d)). The co-operative dynamics of ORF_{tri} is mainly governed by the correlated motions of CC in all chains. The CC domain expresses cooperative motions with RRM domain of chains B and C. The CTD in each monomer expresses anti-cooperative motion with the rest of its domains. At the same time, the CTD also involves in concerted motion with the neighbouring chains (i.e. the CTD of chains A and B moves in accordance with the CC and RRM domains of B and C, respectively).

3.3.1.1. Interactions Stabilizing ORF_{tri}

The trajectory of ORF_{tri} remains more stable when compared to the wild type and mutants. The H-bond between Lys227 and Arg155 fluctuates between 2.8 and 4.5 Å in all the three chains. The inter chain H-bond (Asn157-Tyr152) is stable in AC and BC interface, whereas it is weak in BA interface. The no of H-bonds observed between the interfaces (AC, AB and BC) are variable (Supplementary Table 1) and hence, Q147A-D151A-K154A mutant favours the asymmetric behaviour as in ORF_{wt}. The triple mutants influence the interaction of

CC with hinge 2 and hence promote variable displacements of both CTD and linker (hinge 2). Due to Q147A-D151A-K154A mutations, the interaction between residues of α 3N helix (Ser254, Thr257) and CC domain are absent in ORF_{tri}.

It is revealed from the analysis of ORF_{wt} that the hinge 2-CC interactions are disrupted during the lifting motion of CTD. In the case of ORF_{tri}, the hinge2-CC interactions are absent and hence, the CTD could undergo a free dynamics (colored purple in Figure 3). In ORF_{tri}, the CTD of chain A expresses a slight lifting motion associated with a decrease in angle ($< 10^\circ$) and forms a H-bond between Glu256 and Arg141. A similar lifting motion is also observed in chain B, though the interaction Glu256-Arg141 is highly disturbed. On the other hand, the Glu256-Ser145 H-bond interaction is maintained for about 40 ns in chain C. The H-bond between Arg261 and Pro283 is stable in both chains A and B, while it is disturbed in chain C during initial 30 ns (shown in Figure 9(c)).

It is observed that, the π -interaction between Tyr282 and Arg155, which controls CTD dynamics, is disturbed in chains A and B and remains stable in chain C (Figure 8.I(c)). Also, Tyr282 forms a stable H-bond with Asp252 in both chains A and B as seen in ORF₂₆₁. In addition to this, a π -interaction is formed between Tyr282 and Lys227, which prevents the lifting of CTD in both chains A and B (Figure 8.I(c)). The slight lifting of CTD observed in these chains occurs when Tyr282 interaction shifts from Arg155 (CC) to Lys227 (RRM). The α 3N of both A and B chains relocate away from the CC axis, while in chain C, it moves towards the CC of chain A and form a stable H-bond between Glu143 and Ser145. Also, Tyr282 and Arg155 interaction becomes perfectly planar, where the Tyr282 is positioned to interact strongly with Glu148 (CC) instead of Asp151. All these interactions stabilize the α 3N in chain C and the lifting motion observed from Figure 4.II(b) originates only from the CTD core. This is also reinforced by the hinge residues (hinge 2 and α 3N) predicted by

DynDom (Table 1). All these analyses emphasize the importance of hinge 2-CC interactions in facilitating the functional dynamics of ORF1p.

4. Discussion

Overall, the dynamics of trimeric ORF1p is strongly influenced by the CTD, which adopts distinct structural states such as lifting, twisting and resting during dynamics. All these states are explicitly revealed by the dynamics of ORF_{wt}, whereas the other studied systems expressed these states either individually or in combination. The π -stacking interaction between Tyr282 and Arg155 is proven to be a major contributor in regulating the CTD dynamics¹⁴. CTD can express proper lifting state due to the leverage provided by hinge 2-CC interactions and stabilizes by intra- and inter-chain H-bond interactions with CC rather than hinge 2. On the other hand, the presence of hinge 2-CC interactions and the absence of Tyr282-Arg155 π -stacking interaction leads to the twisting of CTD. Additionally, Tyr282 interacts with the nearby residues such as Val251 (RRM) and Asp151 (CC), which also regulates the CTD dynamics. The H-bond between Arg261 and Pro283 helps to maintain the structural integrity of CTD¹⁴. R261A mutation disrupts this H-bond and releases the CTD core from α 3N. The present analysis also emphasizes this observation and hence the CTD of ORF₂₆₁ shows a free rotation. In spite of the absence of H-bond between Arg261 and Pro283, the H-bonds formed by Tyr282 with Asp252 and Asp151 stabilize the CTDs in ORF₂₆₁. Similarly, in ORF_{tri}, when the hinge 2-CC interactions are absent, the lifting motion of CTDs is perturbed by interaction of Tyr282 with Asp252, Lys227 and Glu148. Though the CTDs of mutated systems (ORF₂₆₁ and ORF_{tri}) does not experience native dynamics (as observed in ORF_{wt}), they are stabilized and retained intact with CC by Tyr282 interactions. The central role of Tyr282 in maintaining the structure of ORF1p is clearly highlighted in ORF₂₈₂ simulations, in which, the CTDs move away from the CC. It can be presumed from this study

that, the overall dynamics of trimeric ORF1p trimer is characterized by various states of CTD and governed by the interactions mediated by Tyr282.

5. Conclusion

The present analyses highlight the structural dynamics of ORF1p in its trimeric state. The CTD of all three chains express various motions such as lifting, twisting and resting, which are regulated by H-bond and π -stacking interactions. In addition to these reported interactions, the present study also discloses the key role of Tyr282 and its interaction with other domains (CC and RRM) in regulating the CTD dynamics. Molecular dynamics simulation studies on mutated systems such as R261A, Y282A and Q147A-D151A-K154A were performed to explore the importance of these residues in maintaining the functional state of ORF1p. It is interesting to observe the oscillatory motions of CTD due to R261A mutation, while in ORF₂₈₂ (Y282A), the CTD move away from the trimeric CC. The absence of interactions between hinge2 and CC (ORF_{tri}) leads to the displacement of CTD and RRM-CTD linker either towards or away from CC. This study provides a clear insight into the functional dynamics of ORF1p mediated by various important residues among which Tyr282 was found to be significant. The native dynamics of CTD (involving lifted, twisted and resting motions) is expected to facilitate the nucleic acid binding and formation of RNP. The lifting motion of CTD opens the RRM-CTD cleft and exposes the positively charged residues for nucleic acid binding, which is followed by the twisting or rotational motions to wrap the nucleic acid around the trimer. Also, the resting position of CTD might render the basic patch residues in CC to be accessible for further nucleic acid binding. Overall, this study provides vital information to unravel the mechanism of RNP formation in TPRT pathway.

Acknowledgements

One of the Authors, Ramaswamy Amutha acknowledges Science and Engineering Research Board, India and University Grants Commission for providing computational facilities in the form of Research Projects.

References

1. R. K. Slotkin and R. Martienssen, *Nature reviews. Genetics*, 2007, **8**, 272-285.
2. C. R. Beck, J. L. Garcia-Perez, R. M. Badge and J. V. Moran, *Annual review of genomics and human genetics*, 2011, **12**, 187-215.
3. G. J. Cost, Q. Feng, A. Jacquier and J. D. Boeke, *The EMBO journal*, 2002, **21**, 5899-5910.
4. A. F. Scott, B. J. Schmeckpeper, M. Abdelrazik, C. T. Comey, B. O'Hara, J. P. Rossiter, T. Cooley, P. Heath, K. D. Smith and L. Margolet, *Genomics*, 1987, **1**, 113-125.
5. S. E. Holmes, M. F. Singer and G. D. Swergold, *The Journal of biological chemistry*, 1992, **267**, 19765-19768.
6. J. V. Moran, S. E. Holmes, T. P. Naas, R. J. DeBerardinis, J. D. Boeke and H. H. Kazazian, Jr., *Cell*, 1996, **87**, 917-927.
7. V. O. Kolosha and S. L. Martin, *The Journal of biological chemistry*, 2003, **278**, 8112-8117.
8. S. L. Martin and F. D. Bushman, *Molecular and cellular biology*, 2001, **21**, 467-475.
9. S. L. Martin, *Journal of biomedicine & biotechnology*, 2006, **2006**, 45621.
10. S. L. Martin, D. Branciforte, D. Keller and D. L. Bain, *Proceedings of the National Academy of Sciences of the United States of America*, 2003, **100**, 13815-13820.

11. K. Januszyk, P. W. Li, V. Villareal, D. Branciforte, H. Wu, Y. Xie, J. Feigon, J. A. Loo, S. L. Martin and R. T. Clubb, *The Journal of biological chemistry*, 2007, **282**, 24893-24904.
12. K. E. Callahan, A. B. Hickman, C. E. Jones, R. Ghirlando and A. V. Furano, *Nucleic acids research*, 2012, **40**, 813-827.
13. J. L. Goodier, L. Zhang, M. R. Vetter and H. H. Kazazian, Jr., *Molecular and cellular biology*, 2007, **27**, 6469-6483.
14. E. Khazina, V. Truffault, R. Buttner, S. Schmidt, M. Coles and O. Weichenrieder, *Nature structural & molecular biology*, 2011, **18**, 1006-1014.
15. E. Khazina and O. Weichenrieder, *Proceedings of the National Academy of Sciences of the United States of America*, 2009, **106**, 731-736.
16. M. D. Hartmann, O. Ridderbusch, K. Zeth, R. Albrecht, O. Testa, D. N. Woolfson, G. Sauer, S. Dunin-Horkawicz, A. N. Lupas and B. H. Alvarez, *Proceedings of the National Academy of Sciences of the United States of America*, 2009, **106**, 16950-16955.
17. H. Hohjoh and M. F. Singer, *The EMBO journal*, 1997, **16**, 6034-6043.
18. S. Basame, P. Wai-lun Li, G. Howard, D. Branciforte, D. Keller and S. L. Martin, *Journal of molecular biology*, 2006, **357**, 351-357.
19. S. L. Martin, *RNA biology*, 2010, **7**, 706-711.
20. S. L. Martin, M. Cruceanu, D. Branciforte, P. Wai-Lun Li, S. C. Kwok, R. S. Hodges and M. C. Williams, *Journal of molecular biology*, 2005, **348**, 549-561.
21. R. Huber, *Nature*, 1979, **280**, 538-539.
22. K. Teilum, J. G. Olsen and B. B. Kragelund, *Cellular and molecular life sciences : CMLS*, 2009, **66**, 2231-2247.
23. M. Falconi, L. Parrilli, A. Battistoni and A. Desideri, *Proteins*, 2002, **47**, 513-520.

24. B. K. Shoichet, W. A. Baase, R. Kuroki and B. W. Matthews, *Proceedings of the National Academy of Sciences of the United States of America*, 1995, **92**, 452-456.
25. G. Dodson and C. S. Verma, *Cellular and molecular life sciences : CMLS*, 2006, **63**, 207-219.
26. G. G. Dodson, D. P. Lane and C. S. Verma, *EMBO reports*, 2008, **9**, 144-150.
27. S. Balasubramanian, M. Rajagopalan and A. Ramaswamy, *Journal of biomolecular structure & dynamics*, 2012, **29**, 659-670.
28. P. Saravanan, V. K. Dubey and S. Patra, *Journal of molecular modeling*, 2014, **20**, 2501.
29. P. Chandrasekaran and R. Rajasekaran, *Molecular bioSystems*, 2014, **10**, 1869-1880.
30. M. Falconi, S. Biocca, G. Novelli and A. Desideri, *BMC structural biology*, 2007, **7**, 73.
31. B. Sangeetha, R. Muthukumaran and R. Amutha, *Journal of computer-aided molecular design*, 2015.
32. D. A. Case, T. A. Darden, T. E. Cheatham, C. L. Simmerling, J. Wang, R. E. Duke, R. Luo, R. C. Walker, W. Zhang, K. M. Merz, B. Roberts, S. Hayik, A. Roitberg, G. Seabra, J. Swails, A. W. Goetz, I. Kolossváry, K. F. Wong, F. Paesani, J. Vanicek, R. M. Wolf, J. Liu, X. Wu, S. R. Brozell, T. Steinbrecher, H. Gohlke, Q. Cai, X. Ye, J. Wang, M. J. Hsieh, G. Cui, D. R. Roe, D. H. Mathews, M. G. Seetin, R. Salomon-Ferrer, C. Sagui, V. Babin, T. Luchko, S. Gusarov, A. Kovalenko and P. A. Kollman, University of California, San Francisco, 2012.
33. V. Hornak, R. Abel, A. Okur, B. Strockbine, A. Roitberg and C. Simmerling, *Proteins*, 2006, **65**, 712-725.
34. W. L. Jorgensen, J. Chandrasekhar, J. D. Madura, R. W. Impey and M. L. Klein, *The Journal of Chemical Physics*, 1983, **79**, 926-935.

35. T. Darden, D. York and L. Pedersen, *The Journal of Chemical Physics*, 1993, **98**, 10089-10092.
36. R. J. Loncharich, B. R. Brooks and R. W. Pastor, *Biopolymers*, 1992, **32**, 523-535.
37. J.-P. Ryckaert, G. Ciccotti and H. J. C. Berendsen, *Journal of Computational Physics*, 1977, **23**, 327-341.
38. D. R. Roe and T. E. Cheatham, *Journal of Chemical Theory and Computation*, 2013, **9**, 3084-3095.
39. T. Ichiye and M. Karplus, *Proteins*, 1991, **11**, 205-217.
40. W. Humphrey, A. Dalke and K. Schulten, *Journal of molecular graphics*, 1996, **14**, 33-38, 27-38.
41. S. Hayward, *Proteins*, 1999, **36**, 425-435.
42. S. Hayward and H. J. Berendsen, *Proteins*, 1998, **30**, 144-154.

Table 1. DynDom-extracted relative motions of the moving domains with respect to the fixed domain

	Fixed domain			Moving domain			Binding residues		
	Chain A	Chain B	Chain C	Chain A	Chain B	Chain C	Chain A	Chain B	Chain C
ORF_{wt}	114-251	114 [^] -253 [^]	114 ^{^^} -262 ^{^^}	255-323	264 [^] -323 [^]	266 ^{^^} -323 ^{^^}	252-254	254 [^] -263 [^]	263 ^{^^} -265 ^{^^}
ORF₂₆₁	114-253	114 [^] -252 [^]	114 ^{^^} -260 ^{^^}	256-323	255 [^] -323 [^]	264 ^{^^} -323 ^{^^}	254-255	253 [^] -254 [^]	261 ^{^^} -262 ^{^^}
ORF₂₈₂	114-254	114 [^] -249 [^]	114 ^{^^} -250 ^{^^}	257-323	263 [^] -323 [^]	261 ^{^^} -323 ^{^^}	255-256	250 [^] -262 [^]	251 ^{^^} -260 ^{^^}
ORF_{tri}	114-251	114-147 [^] , 154 [^] -250 [^]	114 ^{^^} -252 ^{^^}	254-323	258 [^] -323 [^]	259 ^{^^} -323 ^{^^}	252-253	148 [^] -153 [^] , 251 [^] -257 [^]	253 ^{^^} -258 ^{^^}

Figure 1. The structure of ORF1p in trimeric form. In chain A, the secondary structures are labeled and the domains CC, RRM, CTD and hinges are colored in blue, magenta, orange and green, respectively. The inset shows the location of important residues analyzed in the present study. The $C\alpha$ -atoms of the reference residues that are used to calculate the angles and dihedrals to elucidate dynamics of CTD are shown as grey spheres

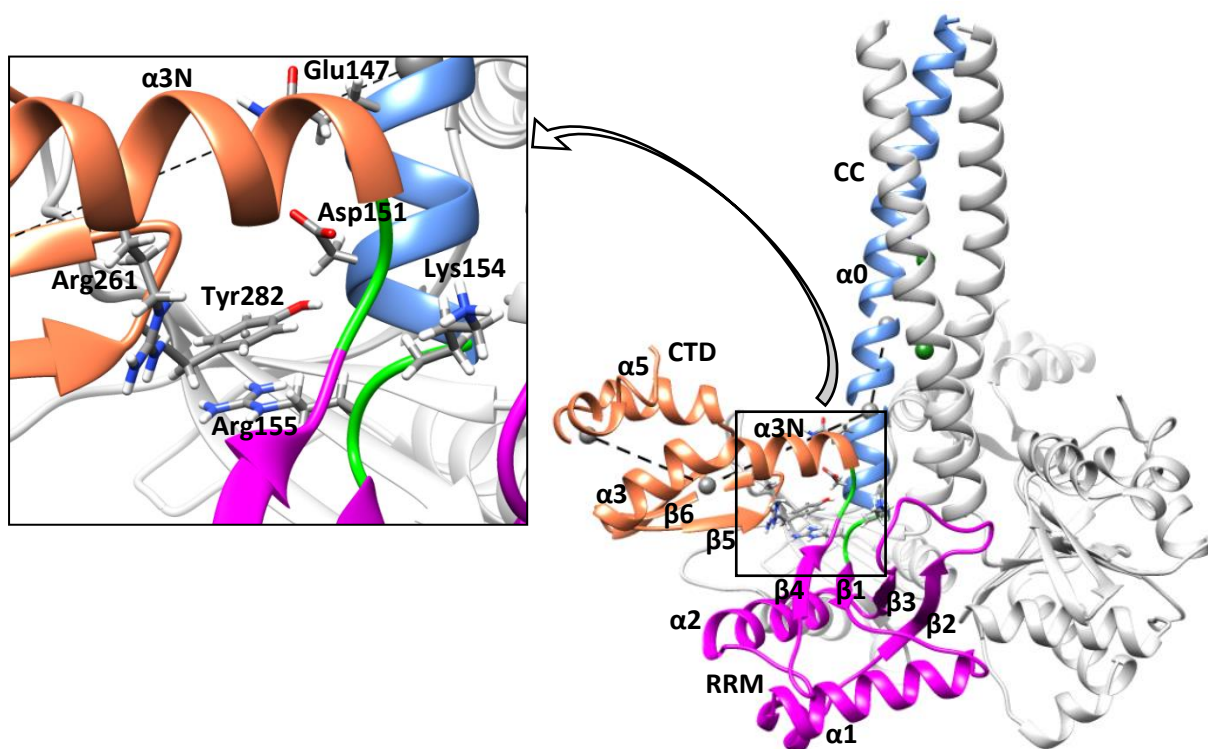


Figure 2. The RMS deviation (a), RMS fluctuation (b) and radius of gyration (c) of ORF_{wt} (black), ORF₂₆₁ (red), ORF₂₈₂ (green) and ORF_{tri} (blue)

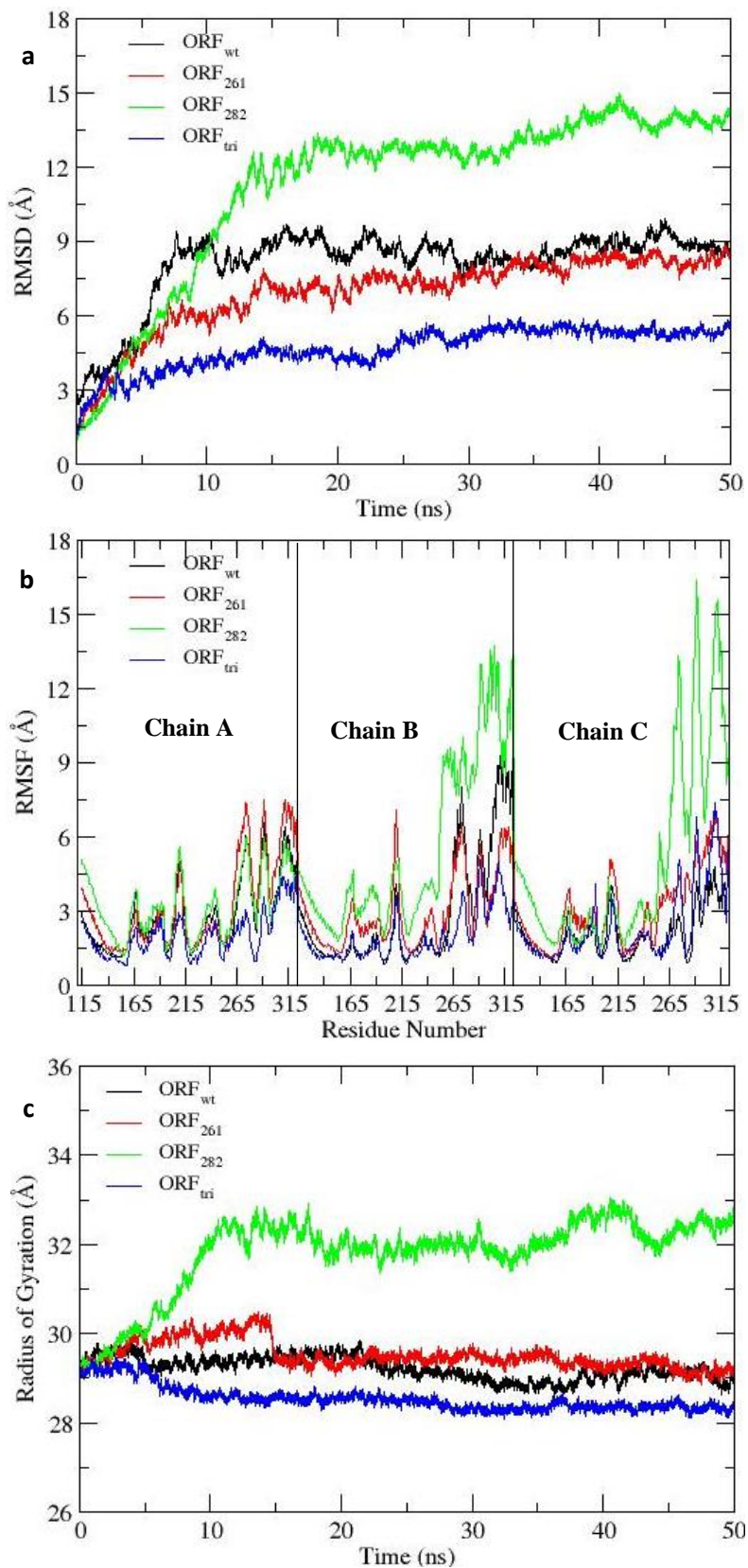


Figure 3. Structural dynamics observed in ORF1p trimer. Superimposition of initial (colored in grey) and final (after 50 ns simulation) conformations of all three chains (A, B and C, respectively) in ORF_{wt} (blue), ORF₂₆₁ (light blue), ORF₂₈₂ (magenta), and ORF_{tri} (purple)

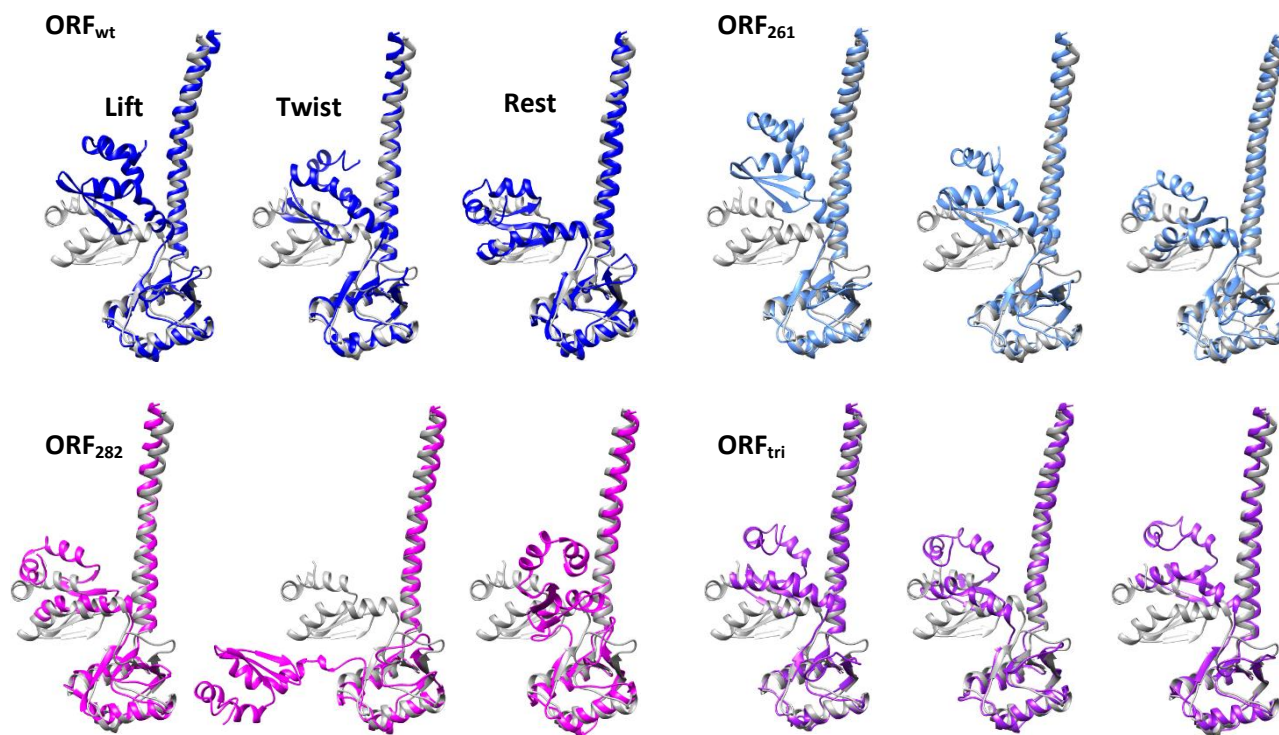


Figure 4. Variation in the angle between CC and CTD monitored using residues (Arg138, Ser145 and Leu286) of chain A (black), B (red) and C (green) in ORF_{wt} (a), ORF₂₆₁ (b), ORF₂₈₂ (c) and ORF_{tri} (d)

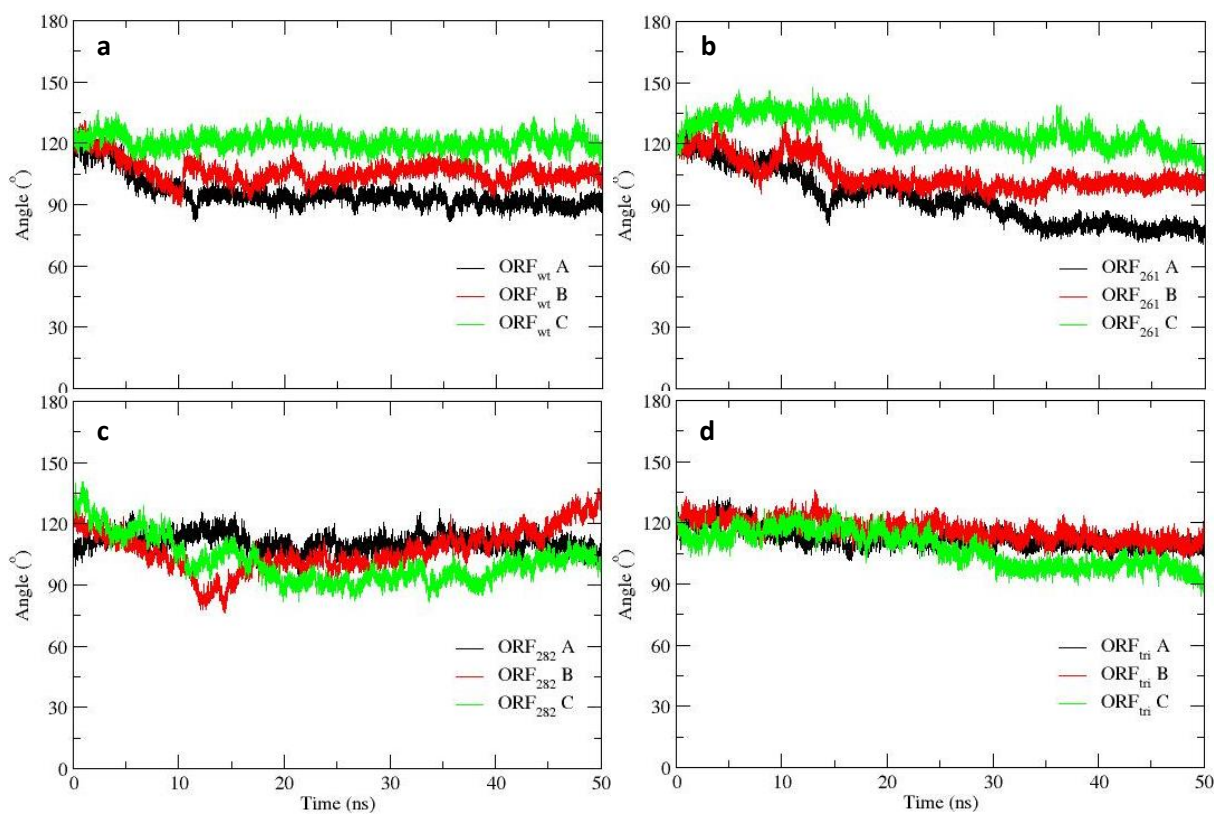


Figure 5. Variation in the dihedral angle between CC and CTD monitored using residues (Arg138, Ser145, Leu286 and Leu313) of chain A (black), B (red) and C (green) in ORF_{wt} (a), ORF₂₆₁ (b), ORF₂₈₂ (c) and ORF_{tri} (d)

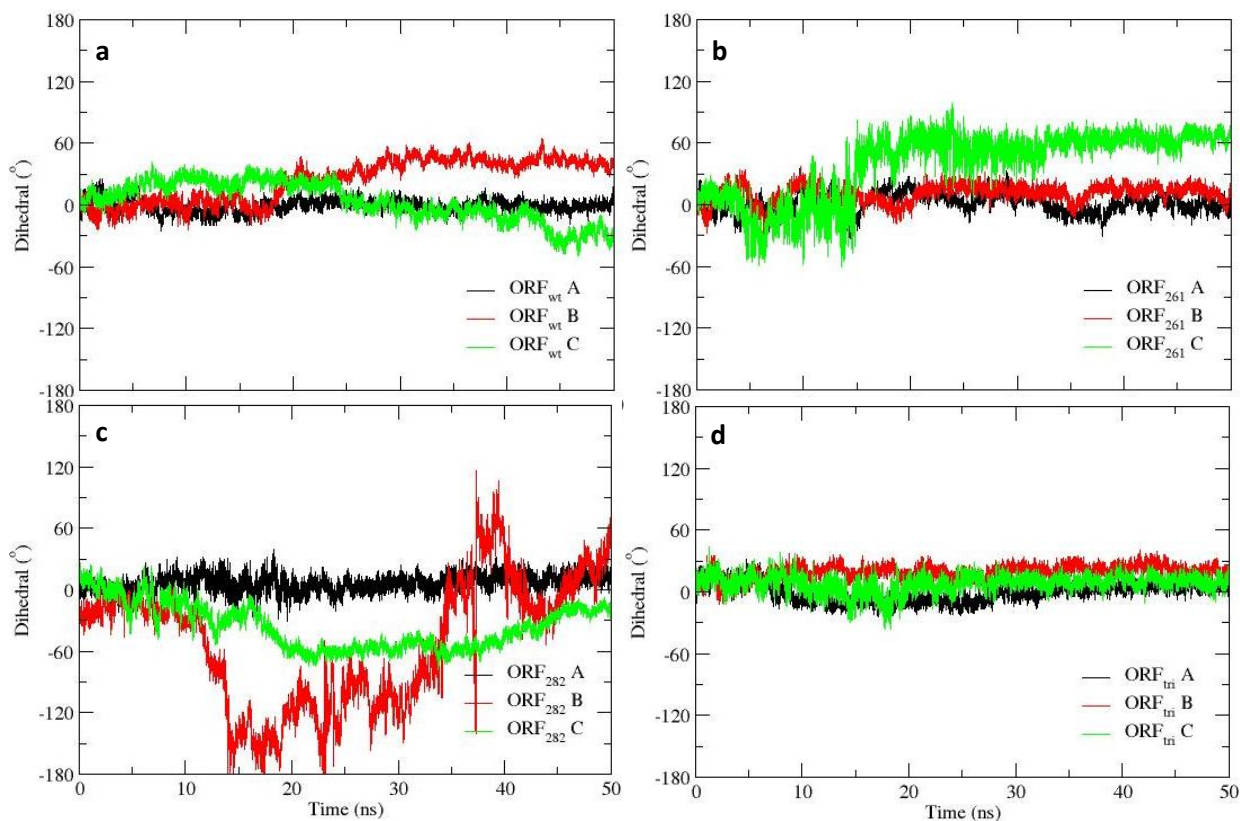


Figure 6. The direction of motion along PC1 is depicted in all the chains of ORF_{wt} (a), ORF₂₆₁ (b), ORF₂₈₂ (c), and ORF_{tri} (d), where the arrows indicate the direction as well as the amplitude of motion. The flexibility is shown in a color coded fashion from blue (rigid) to red (flexible)

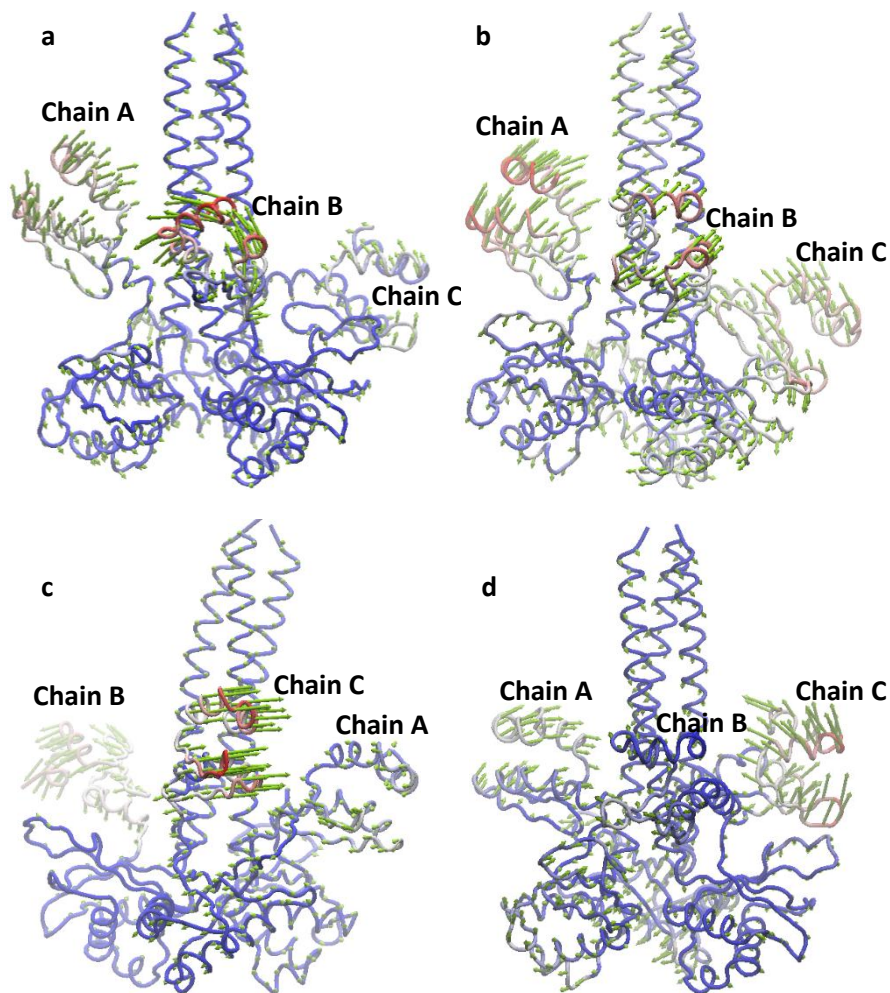


Figure 7. The cross-correlation matrix of ORF_{wt} (a), ORF₂₆₁ (b), ORF₂₈₂ (c) and ORF_{tri} (d) are shown. Positive and negative correlated regions are colored Black and blue shades. The three monomers are differentiated with green, red and orange boxes in the xy-axis

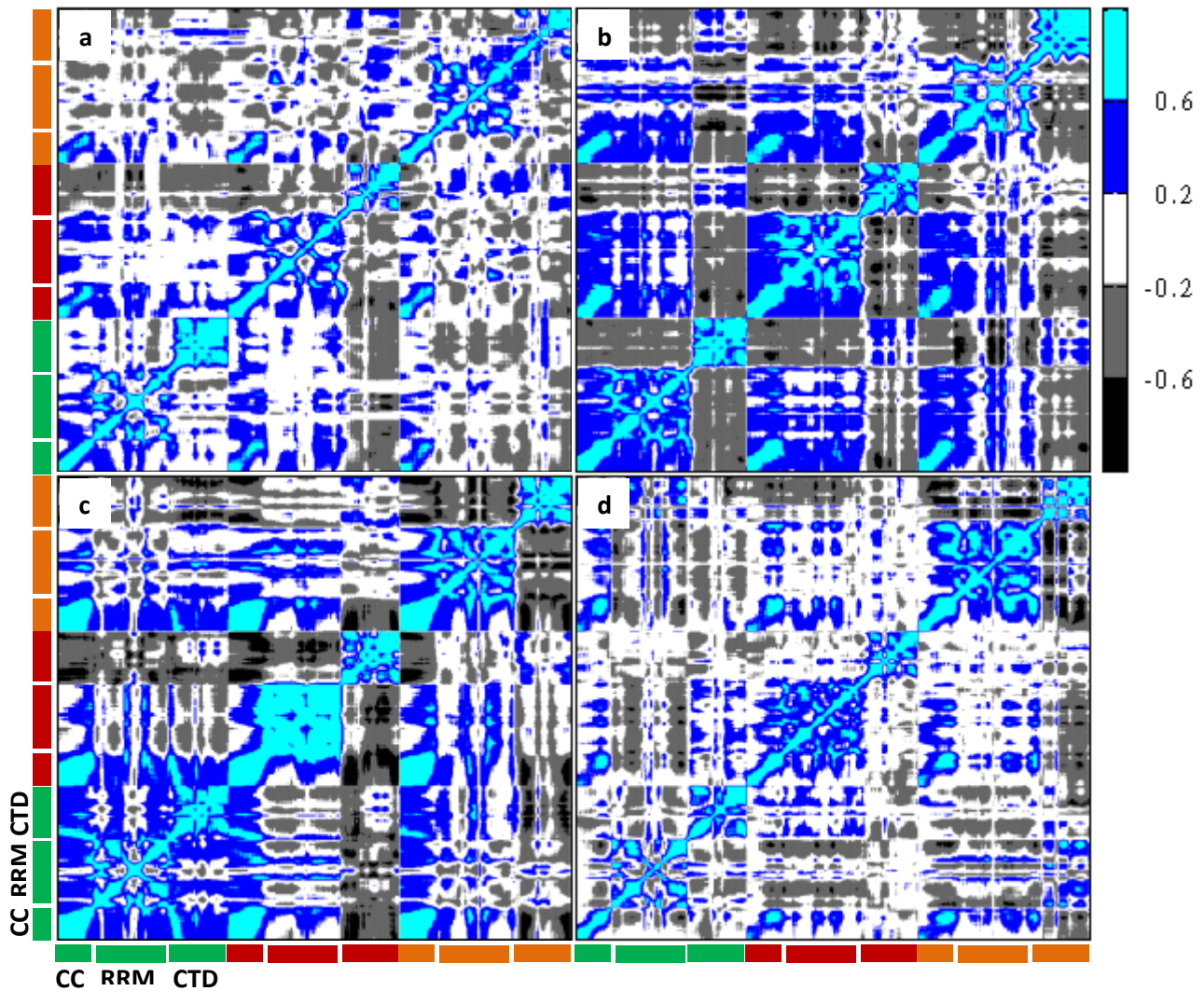


Figure 8. Variation in the π (I) and H-bond (II) distance between Tyr282 and its interacting residues of chain A (black), B (red) and C (green) in ORF_{wt} (a), ORF₂₆₁ (b), and ORF_{tri} (c), respectively

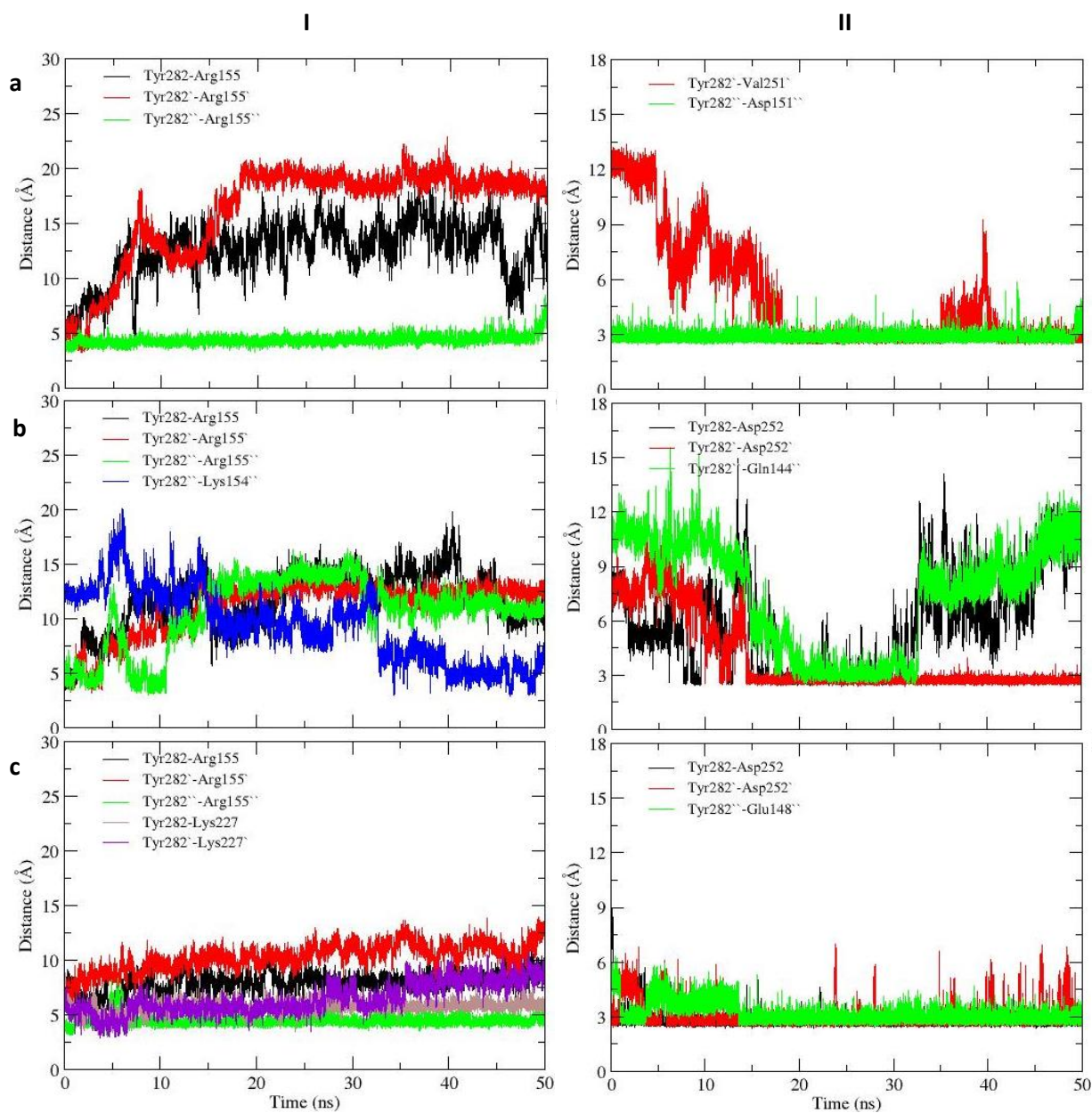


Figure 9. Variation in the H-bond distance between Arg261 and Pro283 of chain A (black), B (red) and C (green) in ORF_{wt} (a), ORF₂₈₂ (b), and ORF_{tri} (c), respectively

